Wang *et al. Biochar* (2026) 8:52
https://doi.org/10.1007/s42773-025-00568-7

Biochar

ORIGINAL RESEARCH Open Access

Biochar-loaded AM fungi coupled with *Arundo donax* enable targeted red mud remediation via valency—specific metal detoxification and soil function recovery

Xiaohui Wang[1], Yingqiang Sun[1,2], Danjuan Zeng[1], Chuanming Fu[1], Keyi Wang[1], Junbo Yang[1], Jianxiong Liao[1], Kanghua Xian[1], Fuqiang Song[3*†] and Gaozhong Pu[1*†]

Abstract

Red mud, a saline-alkaline and metal-contaminated byproduct, poses severe ecological risks. This study elucidates the synergistic remediation mechanisms of biochar (BC) combined with arbuscular mycorrhizal fungi (AMF) in an *Arundo donax*-soil system. We specifically investigated biochar loaded with *Funneliformis mosseae* (BC–FM) and that loaded with *Rhizophagus intraradices* (BC–RI). The BC–FM treatment significantly enhanced the plant antioxidant system and photosynthetic capacity while reducing the content of exchangeable arsenic (As) and soil pH, thereby inducing a "photosynthesis enhancement-As immobilization" synergy. In contrast, the BC–RI treatment markedly increased plant biomass and soil microbial α–diversity, while simultaneously reducing the contents of soil lead (Pb) and sodium ions (Na^+) and enhancing alkaline phosphatase activity—thus demonstrating a "Pb fixation–microbial diversity–soil phosphorus (P) activation" cascade. Rhizosphere network analysis identified key bacterial genera, with *Longimicrobiaceae* driving soil organic carbon accumulation in the BC–FM treatment and *Lechevalieria* enhancing alkaline phosphatase (ALP) activity in the BC–RI treatment. These findings support a novel "fungal species–heavy metal valency matching" principle, where RI preferentially targets cationic Pb, while FM targets anionic As. This principle establishes a three-dimensional synergistic model: "Heavy metal transformation–concurrent salinity-alkalinity mitigation–microbial function activation". The results provide a foundational strategy for zonal red mud remediation: applying BC–RI in Pb–dominated areas and BC–FM in As–contaminated areas.

Highlights

- Proposed "Fungal species–metal valency matching" enables zonal RM remediation: BC–RI for Pb, BC–FM for As.
- The BC–FM synergy boosts photosynthesis and immobilizes As (V), thereby alleviating saline-alkali stress.
- BC–RI enhances biomass, immobilizes Pb, diversifies the microbiota, and activates P.

†Fuqiang Song and Gaozhong Pu have contributed equally as corresponding authors.

*Correspondence:
Fuqiang Song
0431sfq@163.com
Gaozhong Pu
pukouchy@163.com
Full list of author information is available at the end of the article

Springer

- Rhizosphere microbial networks reveal key genera *(Longimicrobiaceae, Lechevalieria)* driving C accumulation and ALP enhancement.

Keywords Biochar-based inoculation, Co-contaminated soil, Salinity-alkalinity stress, Heavy metal toxicity, *Arundo donax*

Graphical Abstract

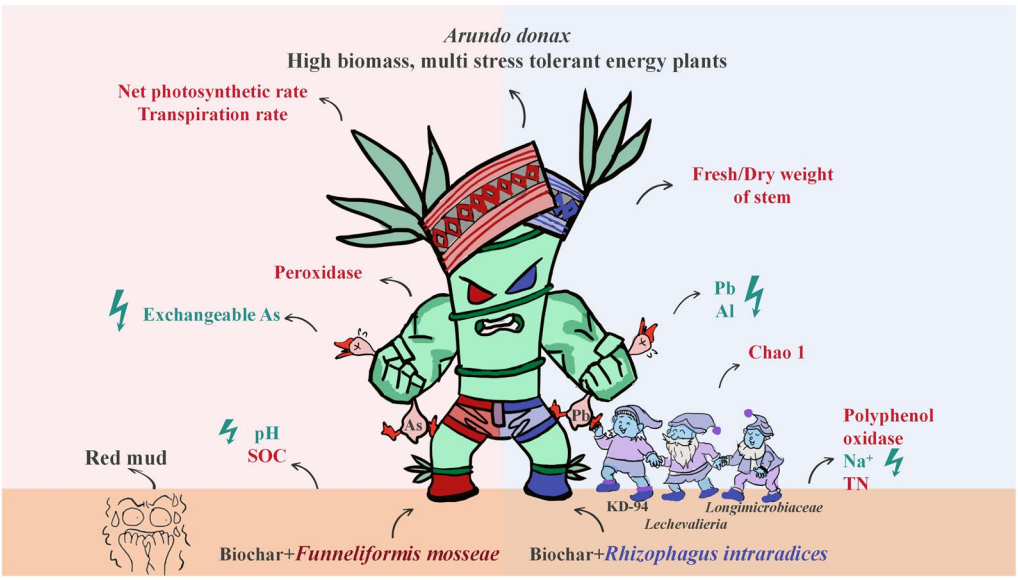

1 Introduction

Red mud (RM) is a highly alkaline and saline residue generated during alumina production, characterized by elevated levels of potentially toxic elements (PTEs) such as cadmium (Cd), arsenic (As), and lead (Pb) (Li et al. 2024). Its large-scale storage poses significant environmental risks due to the potential for contaminants to leach into soil and groundwater, necessitating the development of effective and sustainable remediation strategies (Sarathambal et al. 2017; Di et al. 2019a, b). While phytoremediation using tolerant plants offers an eco-friendly solution, the extreme polymetallic-alkaline-saline stress in RM severely inhibits plant growth and remediation efficiency.

The giant reed (*Arundo donax*) presents a promising candidate for RM phytoremediation due to its high biomass production, deep root system, and documented tolerance to combined heavy metal and salinity stress (Alshaal et al. 2013; Zhang et al. 2021; Tóth et al. 2024). Preliminary studies by our research group have confirmed its ability to complete its life cycle under extreme RM conditions. However, RM's extreme polymetallic-alkaline-saline stress severely inhibits plant growth, biomass production, root development, and remediation efficiency (Wang et al. 2025). Therefore, the success of phytoremediation in such a hostile matrix requires synergistic approaches to enhance plant resilience and soil functionality.

Arbuscular mycorrhizal fungi (AMF) form symbiotic associations with most terrestrial plants, enhancing host stress tolerance by improving nutrient (e.g., phosphorus) and water acquisition (Deng et al. 2025). Specific AMF species, such as *Funneliformis mosseae* (FM) and *Rhizophagus intraradices* (RI), have demonstrated distinct capabilities in contaminated environments (Zhang et al. 2022). FM is known for secreting glomalin-related soil proteins that can chelate metals (Liu et al. 2025a, b), while RI can enhance plant biomass and alter metal bioavailability (Zhu et al. 2024). Nevertheless, AMF performance in RM is often limited by low colonization rates under extreme stress.

Biochar (BC) amendment can create a more favorable microenvironment by adsorbing PTEs, ameliorating pH, and improving soil structure (Rijk et al. 2024; Dou et al. 2024). Crucially, biochar significantly enhances

AMF colonization and activity (Videgain-Marco et al. 2021). Although the combined application of biochar and AMF has shown promise in various contaminated soils (Zaman et al. 2025; Wen et al. 2025), the synergistic mechanisms in the complex and extreme context of RM remain poorly understood. Moreover, the potential for a functional match between specific AMF species and the valence states of predominant contaminants (e.g., anionic AsO_4^{3-} vs. cationic Pb^{2+}) has not been explored. This gap hinders the development of targeted and efficient remediation strategies.

This study introduces a novel "fungal species–heavy metal valence matching" framework to investigate the synergistic remediation of RM using biochar loaded with two distinct AMF species, *Funneliformis mosseae* (BC–FM) and *Rhizophagus intraradices* (BC–RI), in association with *A. donax*. We hypothesize that: (1) BC–FM and BC–RI will differentially enhance plant physiological performance of *A. donax* (photosynthesis, antioxidant defense system, and biomass) under RM stress; (2) the amendments will specifically reduce the mobility and environmental risk of valency-matched PTEs (BC–FM for As and BC–RI for Pb), while concurrently alleviating salinity-alkalinity stress; (3) this targeted approach will restructure the rhizosphere microbial community and upregulate key soil enzymatic activities, leading to improved soil health and function. Our findings aim to provide a mechanistic foundation for a zonal remediation strategy tailored to the specific contaminant profile of RM sites.

2 Materials and methods

2.1 Experimental materials

Tissue-cultured seedlings of giant reed (*A. donax*) were obtained from the Guangxi Institute of Botany (Xian et al. 2018). Seedlings were acclimated in a sand-clay-humus substrate for 30 days (survival rate ≥ 98%) prior to the experiment. Uniform seedlings (wet weight 10 ± 0.5 g) were selected for transplantation.

The arbuscular mycorrhizal fungi (AMF) species *Rhizophagus intraradices* (RI) and *Funneliformis mosseae* (FM) were procured from the Chinese Academy of Agricultural Sciences. Fungal inocula were propagated on maize (*Zea mays* L.) hosts grown in sterilized sand for four months in a greenhouse, with Hoagland nutrient solution supplied every 2–3 days.

Straw-derived biochar (BC) was obtained from Zhengzhou Dingyi Environmental Protection Technology Co., Ltd., with a particle size ranging from 425 to 600 μm. Its basic physicochemical properties were characterized as follows: pH 9.46, soil organic carbon (SOC) 42.21%, total nitrogen (TN) 8.34%, total phosphorus (TP) 2.31%, total potassium (TK) 16.12%, and ash content 7.23%. Prior to inoculation with AMF, the biochar was sterilized by autoclaving at 121 ℃ for 30 min to eliminate indigenous microbial interference.

The red mud (RM) was collected from a disposal site in Pingguo County, Guangxi Zhuang Autonomous Region. Key initial properties of the RM were as follows: pH 10.64, organic matter 3.44 g kg^{-1}, TN 0.18 g kg^{-1}, TP 0.14 g kg^{-1}, sodium ion (Na^+) 20.77 g kg^{-1}, potassium ion (K^+) 2.63 g kg^{-1}, iron (Fe) 276.65 g kg^{-1}, aluminum (Al) 161.01 g kg^{-1}, magnesium (Mg) 5.03 g kg^{-1}, calcium (Ca) 156.69 g kg^{-1}, titanium (Ti) 1.92 g kg^{-1}, arsenic (As) 4.88 g kg^{-1}, cadmium (Cd) 0.67 g kg^{-1}, and lead (Pb) 0.17 g kg^{-1}. The RM was packed into plastic pots (30 cm in diameter × 35 cm in height) for use.

2.2 Experimental design and sampling

A randomized block design was employed with six treatments, each replicated 10 times (n = 10 biological replicates, totaling 60 pots): N (control, no biochar or AMF amendment), BC (biochar only), FM (*Funneliformis mosseae* only), RI (*Rhizophagus intraradices* only), BC–FM (biochar loaded with *Funneliformis mosseae*), and BC–RI (biochar loaded with *Rhizophagus intraradices*).

For AMF-inoculated treatments (FM, RI, BC–FM, BC–RI), a standard inoculum dose of 50 g per pot, containing approximately 1000 viable spores, was thoroughly mixed with the RM. An equivalent amount of sterilized inoculum (including spores, hyphae, and substrate) was added to the non-AMF treatments (N and BC) to ensure a similar microbial background excluding the viable AMF. For biochar-amended treatments (BC, BC–FM, BC–RI), biochar was mixed into the RM at a ratio of 1.5% (w/w).

The pot experiment was conducted in a greenhouse at the Guangxi Institute of Botany from May 17 to October 24, 2023. Pots were periodically repositioned to minimize microclimatic variation. Natural light was utilized throughout the study. Irrigation was adjusted based on plant water requirements to maintain soil moisture without waterlogging.

Photosynthetic parameters were measured in situ during the growing period, and at harvest, plant growth and AMF colonization were assessed. Plants were washed with distilled water and separated into roots, stems, and leaves before storage at −80 ℃ for antioxidant enzyme assays. Rhizosphere soil (loosely attached to roots) and root-adhering soil (firmly attached to roots, collected with a brush) were stored at −20 ℃ and shipped on dry ice for microbiome analysis.

2.3 Plant physiological and growth measurements

In situ photosynthetic parameters, including net photosynthesis (Pn), transpiration rate (Tr), intercellular CO_2 concentration (Ci), and stomatal conductance (Gs),

were measured on three randomly selected plants per treatment between 9:00 and 12:00 on clear days in May, July, and September, using a LI–6400XT portable photosynthesis system (LI–COR, Nebraska, USA, photosynthetically active radiation set to 1000 μmol m^{-2} s^{-1}. Chlorophyll content was assessed with a SPAD–502 (Konica Minolta, Japan) at 9:00 a.m. on clear mornings.

Plant height and basal stem diameter were measured with a ruler and a caliper. Fresh weights of roots, stems, and leaves were determined using an electronic balance (JT3003D). Samples were oven-dried (105 ℃ for 30 min, then 65 ℃ for 48 h) to constant weight.

The colonization and biochar effects of AMF or BC on plant biomass were quantified to evaluate the specific contribution of fungal inoculation or BC to plant growth. The colonization and biochar effects (E) were calculated separately for the FM, RI, and BC treatments using the following formula:

$$E = \frac{B_1 - B_2}{B_1} \quad (1)$$

where B_1 is the average plant biomass in a treatment (FM/RI/BC), and B_2 is the average plant biomass in the corresponding treatment (without FM/RI/BC) but with an equivalent background.

The activities of the antioxidant enzymes catalase (CAT), peroxidase (POD), and superoxide dismutase (SOD) in fresh leaf tissues were determined using commercial assay kits (Nanjing Jiancheng Bioengineering Institute, China) following the manufacturer's protocols (Gao. 2006).

2.4 Pollution level and risk assessment

The total and acid-soluble fractions of As, Cd, and Pb were quantified by inductively coupled plasma mass spectrometry (ICP–MS, Agilent 7700e, USA) following digestion and the BCR sequential extraction procedure, respectively (Cappuyns et al. 2007).

Single-factor pollution index (Pi):

$$Pi = \frac{\text{Measured soil heavy metal concentration}}{\text{heavy metal evaluation standard value}} \quad (2)$$

$Pi < 1$ indicates no pollution, while $Pi > 1$ indicates increasing pollution severity.

Comprehensive pollution index (CPI; Nemerow Index):

$$CPI = \sqrt{\frac{(\frac{1}{n}\sum_{i=1}^{n} Pi)^2 + (\max Pi)^2}{2}} \quad (3)$$

The pollution level is classified as: $CPI \leq 0.7$: clean, $0.7 < CPI \leq 1$: alert level, $1 < CPI \leq 2$: slight pollution, $2 < CPI \leq 3$: moderate pollution, $CPI > 3$: severe pollution.

Risk Assessment Code (RAC):

$$RAC = \frac{\text{Acid} - \text{soluble metal}}{\text{Total metal}} \quad (4)$$

The ecological risk is categorized as: RAC <1%: no risk, 1%<RAC<10%: low, 0% < RAC < 30%: medium, 30% < RAC < 50%: high, RAC > 50%: very high.

2.5 Soil sampling and analysis

Soil pH was measured in a 1:2.5 (w/v) soil–water suspension using a pH meter (PHSJ–3F). Electrical conductivity (EC), salinity, and total dissolved solids (TDS) were measured with conductivity and salinity meters; TDS was estimated as EC × 0.5–0.7. Soil organic carbon (SOC) was determined by dichromate oxidation. TN and TP were measured using the Kjeldahl method and molybdenum–antimony colorimetric method after H_2SO_4 digestion, respectively. Concentrations of Mg, Al, Ca, Ti, and Fe were analyzed using ICP–MS. Concentrations of Na^+ and K^+ were measured by flame photometry.

Soil enzyme activities were assessed as follows: alkaline phosphatase (AKP) by disodium phenyl phosphate colorimetry, catalase (CAT) by UV spectrophotometry based on H_2O_2 consumption, polyphenol oxidase (PPO) using catechol as a substrate, and peroxidase (POD) by guaiacol colorimetry (Robinson et al. 1995).

2.6 Microbial community analysis

Total genomic DNA was extracted from 0.5 g rhizosphere soil using the Omega Mag–bind Soil DNA Kit. The hypervariable V3–V4 region of the bacterial 16S rRNA gene was amplified using primers 338F (5′–ACT CCTACGGGAGGCAGCA–3′) and 806R (5′–GGACTA CHVGGGTWTCTAAT–3′). Amplicon sequencing was performed on the Illumina NovaSeq platform by Panomix Biomedical Technology Co., Ltd. (Suzhou, China).

2.7 Data and statistical analysis

All data were first tested for normality (Shapiro–Wilk test) and homogeneity of variances (Levene's test) prior to statistical analysis. One-way analysis of variance (ANOVA) was performed, and where significant effects were found ($p < 0.05$), Tukey's Honestly Significant Difference (HSD) test was used for post-hoc comparisons. Student's t-test was used for specific pairwise comparisons where appropriate. All statistical analyses were conducted using SPSS Statistics 25. Data presented in figures were transformed using log10 (y + 1) where necessary to meet the assumptions of normality, as indicated in the figure captions.

Microbial community analysis, including alpha diversity (Chao1, Shannon, Simpson indices) and beta diversity (Non-metric Multidimensional Scaling, NMDS, based on

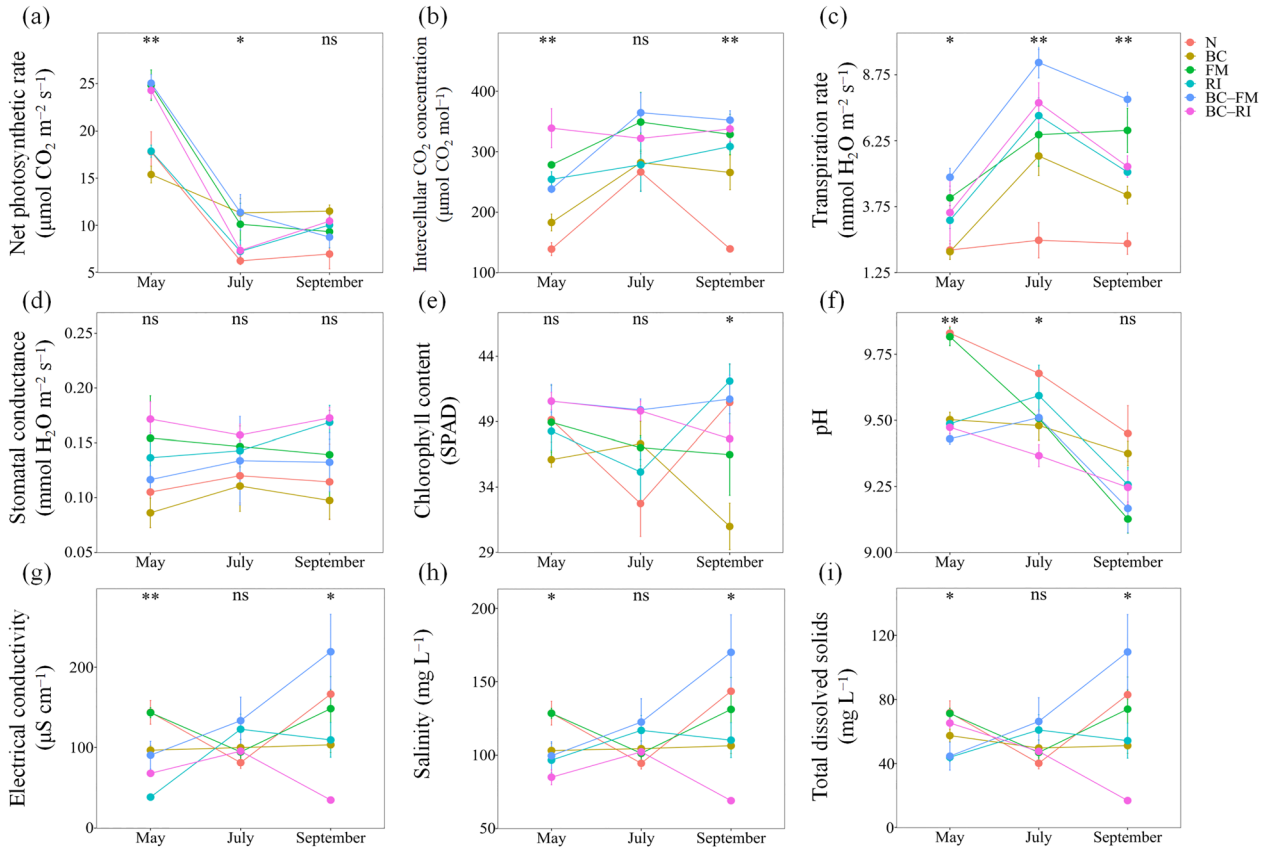

Fig. 1 Temporal variations in **a** net photosynthetic rate (Pn, μmol CO_2 m^{-2} s^{-1}), **b** intercellular CO_2 concentration (Ci, μmol CO_2 mol^{-1}), **c** transpiration rate (Tr, mmol H_2O m^{-2} s^{-1}), **d** stomatal conductance (Gs, mol H_2O m^{-2}·s^{-1}), **e** chlorophyll content (SPAD), and red mud properties: **f** pH, **g** electrical conductivity (EC, μS cm^{-1}), **h** salinity (mg L^{-1}), **i** total dissolved solids (TDS, mg L^{-1}). Treatments: N (control, no biochar or AMF), BC (biochar alone), FM (*Funneliformis mosseae* alone), RI (*Rhizophagus intraradices* alone), BC–FM (biochar + FM), BC–RI (biochar + RI). Significant differences among treatments (Kruskal–Wallis test; *$p < 0.05$, **$p < 0.01$; $n \geq 3$)

Bray–Curtis distance), was performed using QIIME2. Co-occurrence network analysis was constructed at the genus level based on Spearman correlations ($|r| \geq 0.4$, $p < 0.05$). Functional annotation of prokaryotic taxa (FAPROTAX) was used to predict potential biogeochemical cycling functions. The raw sequencing data have been deposited in the NCBI Sequence Read Archive (SRA) under the accession number PRJNA1294589.

3 Result and discussion

3.1 Functional divergence of biochar-loaded AMF in enhancing plant physiological performance

The inoculation with biochar-loaded AMF significantly enhanced the photosynthetic capacity and growth of *A. donax* under red mud stress, with functional divergence observed between the two fungal species (Fig. 1a–e). In the early growth stage (May), both BC–FM and BC–RI treatments achieved peak Pn (25.10 and 24.33 μmol CO_2 m^{-2} s^{-1}), representing increases of over 36% compared to the N treatment ($p < 0.05$). This initial boost can be attributed to the improved nutrient (particularly phosphorus) acquisition facilitated by the extensive extraradical hyphae of AMF, which is crucial for establishing the photosynthetic apparatus (Zheng et al. 2024).

A key differential response was observed in the Ci. BC–RI led to a significantly elevated Ci during early growth (with Ci of 338.88 μmol CO_2 mol^{-1}, 143.92% higher than the N control), suggesting that photosynthetic initiation was initially governed by non-stomatal limitations, potentially due to a lag in the full activation of carbon assimilation enzymes like Rubisco (Liu et al. 2025a, b). This strategy likely prioritized resource allocation to rapid biomass accumulation, as evidenced by BC–RI yielding the highest stem dry weight (4.98 g $plant^{-1}$), which was significantly increased by 128.44% compared to the control (Table S1). This aligns with an ecological strategy of rapid colonization and sustained provisioning by the RI symbiosis.

Conversely, by the late growth stage (September), the BC–FM treatment exhibited the highest Ci (352.24 μmol

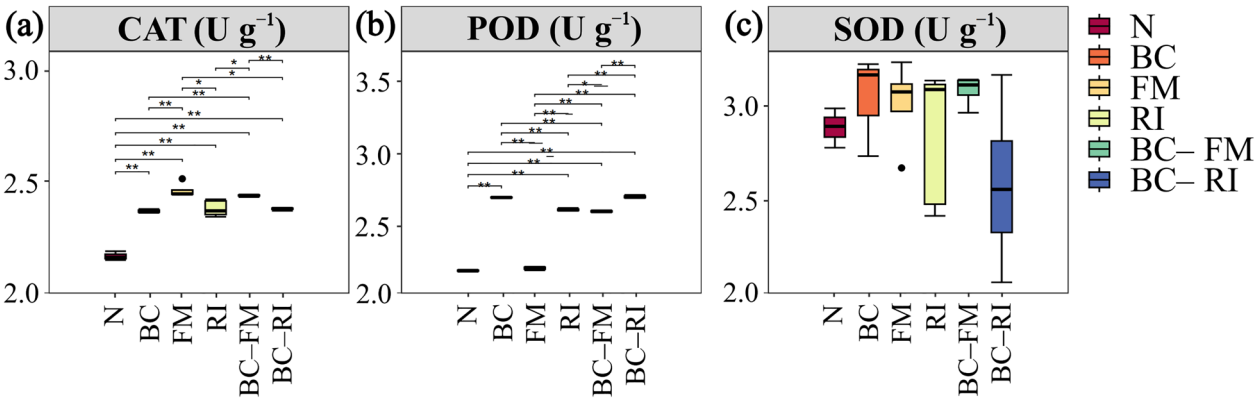

Fig. 2 Antioxidant enzyme activities in *Arundo donax*: **a** catalase (CAT, U g^{-1}), **b** peroxidase (POD, U g^{-1}), **c** superoxide dismutase (SOD, U g^{-1}). Treatments as in Fig. 1. Asterisks denote significant differences between treatments (T-test, *$p < 0.05$, **$p < 0.01$, n ≥ 3)

CO_2 mol^{-1}) and consistently maintained the highest transpiration rate (Tr) throughout the experiment. This indicates a distinct, balanced metabolic strategy where the carbon consumption by FM hyphae potentially increased the demand for CO_2 fixation (Hobbie et al. 2025). Furthermore, FM likely delayed leaf senescence by enhancing leaf antioxidant capacity (Fig. 2), thereby preserving the photosynthetic functionality of leaves. These temporal and functional niche differentiations underscore that the two AMF species employ distinct strategies to enhance plant carbon assimilation under stress, with BC–RI favoring early biomass investment and BC–FM promoting sustained photosynthetic activity.

3.2 AMF-Specific regulation of antioxidant defense systems

The plant's antioxidant defense response was uniquely modulated by the type of AMF inoculation (Fig. 2a–c). The FM–only treatment elicited the highest CAT activity (a 90.5% increase relative to the control), while its POD activity remained low. This suggests a preferential reliance on the CAT-dominated H_2O_2-scavenging pathway in FM-inoculated plants. This response may be linked to the secretion of glomalin-related soil proteins by FM, which could enhance membrane stability and protect enzyme active sites from metal-induced inactivation (Ma et al. 2021; Xie et al. 2025).

In contrast, treatments involving biochar (BC and BC–RI) showed significantly elevated POD activity (Fig. 2b). The "fungus-biochar complementarity" was most evident in the BC–RI treatment, which achieved the peak POD activity (503.40 U g^{-1}) while concurrently reducing leaf Na^+ content (Fig. 3a). This indicates that RI fungi, in synergy with biochar, alleviated osmotic stress, thereby reducing the sustained induction demand for certain antioxidant pathways (Essahibi et al. 2019). The lack of significant difference in SOD activity across all treatments implies that the baseline oxidative stress in RM universally activated this first line of defense to saturation (Babzada et al. 2024). Collectively, these results demonstrate that fungus-loaded biochar amendments mitigate oxidative stress not only by driving heavy metal immobilization (Table 1) but also by orchestrating specific antioxidant enzyme responses to restore cellular homeostasis.

3.3 Valency-specific immobilization of heavy metals and risk mitigation

Pollution assessment confirmed severe heavy metal contamination in the RM (CPI > 3), with a high to very high risk for As (RAC > 30) and a moderate risk for Cd (Table 1). The application of biochar-loaded AMF significantly altered metal mobility, and critically, the responses exhibited a clear fungal strain specificity that aligns with our "fungal species–metal valency matching" hypothesis.

The BC–RI treatment was most effective in mitigating cationic metal risk. It resulted in the lowest total soil Pb (T–Pb), representing a 10.91% reduction compared to the control ($p < 0.05$), and also achieved the lowest comprehensive pollution index (CPI). This reduction is likely linked to RI-mediated phosphate secretion, which induces the precipitation of stable Pb-phosphate minerals. This process simultaneously diminished ROS generation and alleviated mitochondrial electron transport chain damage by reducing apoplastic heavymetal concentrations (Glinska and Gapinska 2013; Seshadri et al. 2015).

Conversely, the BC–FM treatment preferentially mitigated the risk of anionic arsenic. It achieved the lowest level of bioavailable (exchangeable) arsenic (A–As) (15.96 mg kg^{-1}) and the lowest RAC values for As (34.60) (Table 1). It is noteworthy that this reduction in As

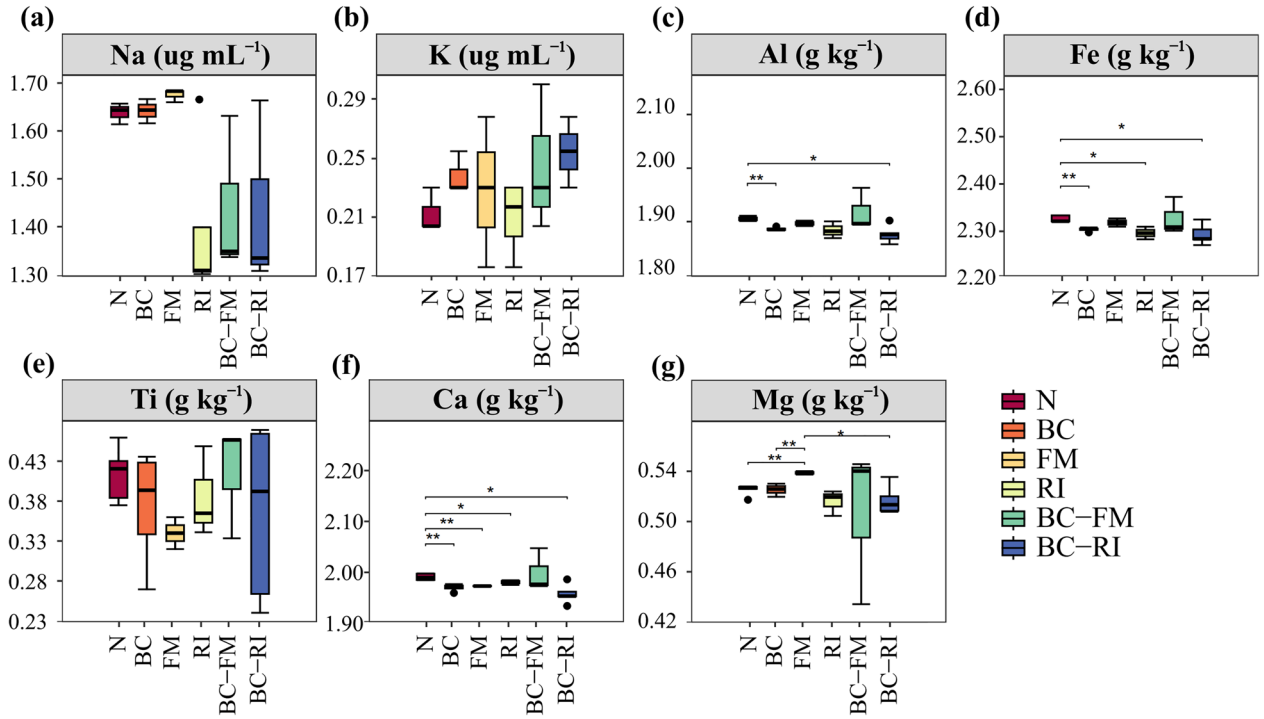

Fig. 3 Concentrations of **a** Na^+, **b** K^+ (μg mL^{-1}), and **c** Al, **d** Fe, **e** Ti, **f** Ca, **g** Mg (g kg^{-1}) in red mud across treatments. Treatments and statistical conventions as in Fig. 2

Table 1 Heavy metal content, pollution indices, and risk assessment in red mud

Parameter	N	BC	FM	RI	BC–FM	BC–RI
T–As (mg kg^{-1})	42.79 ± 0.60 a	32.28 ± 8.49 a	30.37 ± 14.41 a	34.99 ± 15.98 a	46.14 ± 7.33 a	41.05 ± 8.85 a
T–Cd (mg kg^{-1})	6.87 ± 0.39 a	6.31 ± 0.16 a	6.98 ± 0.33 a	6.39 ± 0.63 a	6.91 ± 0.41 a	6.02 ± 0.37 a
T–Pb (mg kg^{-1})	93.60 ± 2.40 ab	88.69 ± 2.33 ab	95.18 ± 0.01 ab	86.34 ± 4.81 b	99.42 ± 9.54 a	83.39 ± 1.34 b
A–As (mg kg^{-1})	17.83 ± 0.86 bc	20.41 ± 2.41 bc	21.04 ± 0.80 b	19.20 ± 0.70 bc	15.96 ± 0.56 c	29.09 ± 3.06 a
A–Cd (mg kg^{-1})	1.31 ± 0.06 a	1.47 ± 0.06 a	1.34 ± 0.19 a	1.38 ± 0.05 a	1.31 ± 0.05 a	1.32 ± 0.13 a
A–Pb (mg kg^{-1})	6.64 ± 0.32 b	8.27 ± 0.41 a	7.62 ± 0.73 ab	7.13 ± 0.68 ab	6.95 ± 0.09 ab	7.13 ± 0.73 ab
Pi–As	1.71 a	1.29 a	1.21 a	1.40 a a	1.85 a	1.64 a
Pi–Cd	11.45 a	10.52 a	11.64 a	10.64 a	11.52 a	10.03 a
Pi–Pb	0.55 a	0.52 a	0.56 a	0.51 a	0.58 a	0.49 a
CPI	8.72 a	7.99 a	8.82 a	8.09 a	8.79 a	7.65 a
RAC–As	41.67 a	63.24 a	69.27 a	54.88 a	34.60 a	70.85 a
RAC–Cd	19.06 a	23.22 a	19.16 a	21.54 a	18.89 a	22.01 a
RAC–Pb	7.10 a	9.32 a	8.01 a	8.25 a	6.99 a	8.55 a

Soil contamination thresholds: As = 25 mg kg^{-1}, Cd = 0.6 mg kg^{-1}, Pb = 170 mg kg^{-1} (Chinese National Standard GB 15618–2018 for agricultural soil risk control). Metal fractions: T–As/Cd/Pb: Total arsenic/cadmium/lead content. A–As/Cd/Pb: Bioavailable (exchangeable) arsenic/cadmium/lead content. Pollution indices: Pi–As/Cd/Pb: Single–factor index for arsenic/cadmium/lead (Pi > 1 indicates pollution). CPI: Comprehensive Nemerow Pollution Index (CPI > 3 indicates severe pollution). RAC: Risk Assessment Code (categorization: < 1% = negligible, 1–10% = low, 10–30% = moderate, 30–50% = high, > 50% = extreme risk). Treatments as in Fig. 1. Different lowercase letters (a, b, c) denote significant differences between treatments (Tukey's HSD test, n ≥ 3)

bioavailability occurred alongside a higher total As content in the BC–FM treatment. This apparent discrepancy underscores a successful remediation outcome: the biochar component likely acts as a sink, adsorbing and retaining As within the soil matrix, thereby increasing the total measured pool. Concurrently, the FM fungi actively transform the arsenic speciation, stabilizing the adsorbed metal into less bioavailable forms through mechanisms:

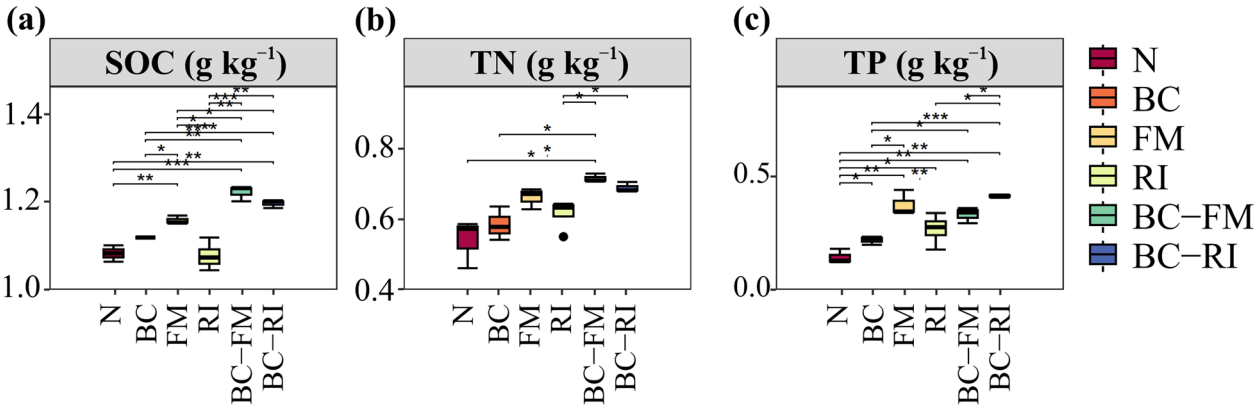

Fig. 4 Rhizospheric **a** soil organic carbon (SOC, g kg^{-1}), **b** total nitrogen (TN, g kg^{-1}), **c** total phosphorus (TP, g kg^{-1}). Treatments and statistical notations as in Fig. 2

(1) secretion of GRSP, which binds or adsorbs arsenic onto hyphal surfaces (Garg and Cheema. 2021; Hao et al. 2024), and (2) the potential activation of sulfur metabolism pathways promoting As sulfide precipitation (Sun et al. 2023). Thus, the BC–FM system effectively sequesters arsenic and reduces its ecotoxicological risk, even if the total concentration remains elevated.

The fundamentally different chemical strategies employed by each fungal-biochar assembly—RI for cationic fixation via precipitation, and FM for anionic immobilization via adsorption and potential re-precipitation—robustly support the valency-specific detoxification model. While direct spectroscopic evidence of valence state changes (e.g., via XPS) is a target for future research, the convergent evidence from metal fractionation, risk assessment, and the established biochemistry of the symbionts provides a compelling, multi-faceted validation of our proposed mechanism.

3.4 Synergistic amelioration of red mud physicochemical properties

The combined system effectively ameliorated the hostile physicochemical properties of RM (Fig. 1f–i, 3, 4). A critical finding was the significant reduction in soil pH by the FM and BC–FM treatments (to 9.13 and 9.17, respectively). This is a notable departure from the typical alkalizing effect of biochar alone (Chen et al. 2025a, b) and from the reported synergy of AMF and biochar in acidic soils, where their combined application often aims to elevate soil pH (Nirukshan et al. 2023; Li et al. 2025). In our alkaline RM environment, the observed acidification is likely driven by the AMF component. A postulated mechanism is that AMF can regulate rhizosphere pH by secreting, or inducing the host plant to release, organic acids (e.g., oxalic acid, malic acid) in response to ambient alkalinity (Souza et al. 2025; Feng et al. 2023), thereby creating a more favorable microenvironment for plant growth. This contrast underscores the context-dependent nature of AMF–biochar interactions, where the same combination can exert opposing effects on soil pH in different contamination scenarios. While direct measurement of rhizosphere organic acids remains a focus for future research, the functional importance of this pH reduction is clear, as it directly influences the speciation and bioavailability of heavy metals (Fig. S4), thereby contributing to the overall remediation efficacy.

The BC–RI treatment was particularly effective in reducing salinity-related stress, shown by a 48.63% reduction in sodium ion (Na^+) concentration ($p > 0.05$) along with the lowest final values for electrical conductivity (EC), salinity, and total dissolved solids (TDS) (34 μS cm^{-1}, 19 mg L^{-1}, and 17 mg L^{-1}) (Fig. 1f–i). It also significantly decreased the concentrations of Al (74.22 g kg^{-1}), Fe (191.29 g kg^{-1}), Ca (88.83 g kg^{-1}), and Mg (2.26 g kg^{-1}) in the RM (Fig. 3). The Al content under BC–RI showed particular reduction, decreasing by 53.91% relative to pristine RM (161.01 g kg^{-1}). In contrast, BC–FM exhibited elevated levels of these metal cations, suggesting a dual immobilization mechanism where metal oxides surface-complex arsenate, and FM activity drives arsenic sulfide precipitation, collectively forming a synergistic adsorption–microbial fixation barrier (Zhou et al. 2023).

Both AMF inoculation and biochar application significantly enhanced soil nutrient content (Fig. 4). BC–FM led to the highest accumulation of SOC and TN (16.01 g kg^{-1} and 4.12 g kg^{-1}), likely through fungal secretion of extracellular polysaccharides that stabilize organic matter (Gujre et al. 2021; Chandra et al. 2022). BC–RI, however, recorded the highest TP level (1.59 g kg^{-1}), which can be attributed to the synergistic effect of RI hyphae secreting phosphatases to mobilize phosphorus, while biochar inhibiting P re-immobilization via ion exchange (He

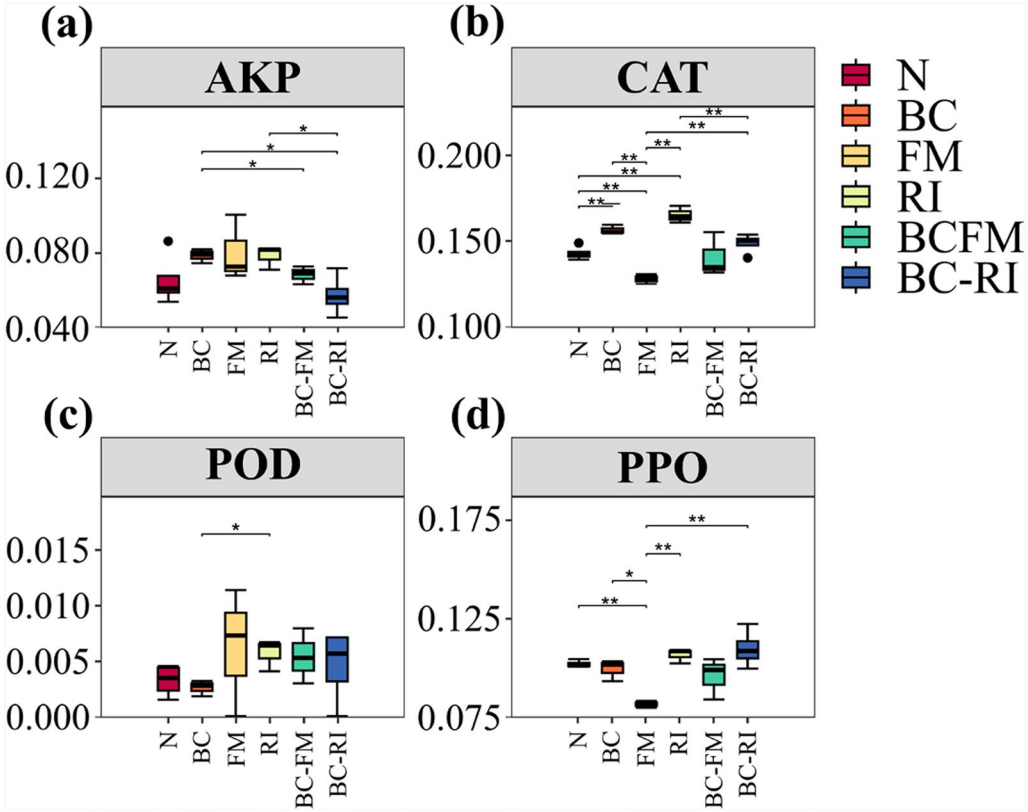

Fig. 5 Soil enzyme activities: **a** alkaline phosphatase (AKP, ΔA min^{-1}), **b** catalase (CAT, ΔA min^{-1}), **c** peroxidase (POD, ΔA min^{-1}), **d** polyphenol oxidase (PPO, ΔA min^{-1}). Treatments and statistical notations as in Fig. 2

et al. 2018; Lang et al. 2021; Yang et al. 2021). FAPROTAX functional prediction analysis (Fig. S3) corroborated this functional divergence, showing that RI primarily enhanced nitrogen cycling functions, while BC–FM boosted carbon cycling pathways.

3.5 Activation of rhizosphere enzyme activities and microbial community restructuring

The treatments differentially activated key soil enzymes, reflecting shifts in microbial functional potential (Fig. 5). The RI treatment exhibited the highest activities of AKP and CAT, underscoring its role in P mobilization and oxidative stress mitigation in the rhizosphere. The BC–RI treatment showed the highest relative activity of PPO, which was 7.92% higher than that in the N treatment (Fig. 5). This RI–biochar interaction is critical as it establishes a dynamic "demand–supply" balance for phosphorus and enhances the detoxification of reactive oxygen species (ROS) (Zhang et al. 2022; Li et al. 2023 Yang et al. 2025).

The sequencing depth was assessed and deemed sufficient for the downstream diversity (alpha and beta) and network analyses conducted in this study, in accordance with standard practices in microbial ecology. Analysis of the rhizosphere bacterial community revealed significant restructuring (Fig. 6). The BC–RI treatment markedly increased bacterial richness (Chao1 index increased by 27.40%, $p < 0.05$) (Fig. 6a–c). NMDS analysis revealed clear separation between communities with and without AMF/biochar amendments (ANOSIM: $R = 0.388$, $p = 0.001$), indicating distinct microbial assemblages (Fig. 6d).

Co-occurrence network analysis further revealed that AMF and biochar amendments generally reduced network complexity (Fig. 7 and S2). Keystone taxa (i.e., nodes with the highest degree) were mainly concentrated in Cluster 1 across all treatments. Based on topological features, three connector taxa were identified as key species in the microbial co-occurrence network: *Salinarimonas*, *Rhizorhapis*, and *Desulfovibrio* (Table S2). AMF and biochar treatments consistently decreased the relative abundance of *Salinarimonas*, while increasing those of *Rhizorhapis* and *Desulfovibrio*. In particular, the BC–FM treatment showed the most pronounced changes: *Salinarimonas* abundance decreased by 93.46%, while *Rhizorhapis* and *Desulfovibrio* increased by 621.74% and 3192.86%, respectively, relative to the N treatment, the latter being a

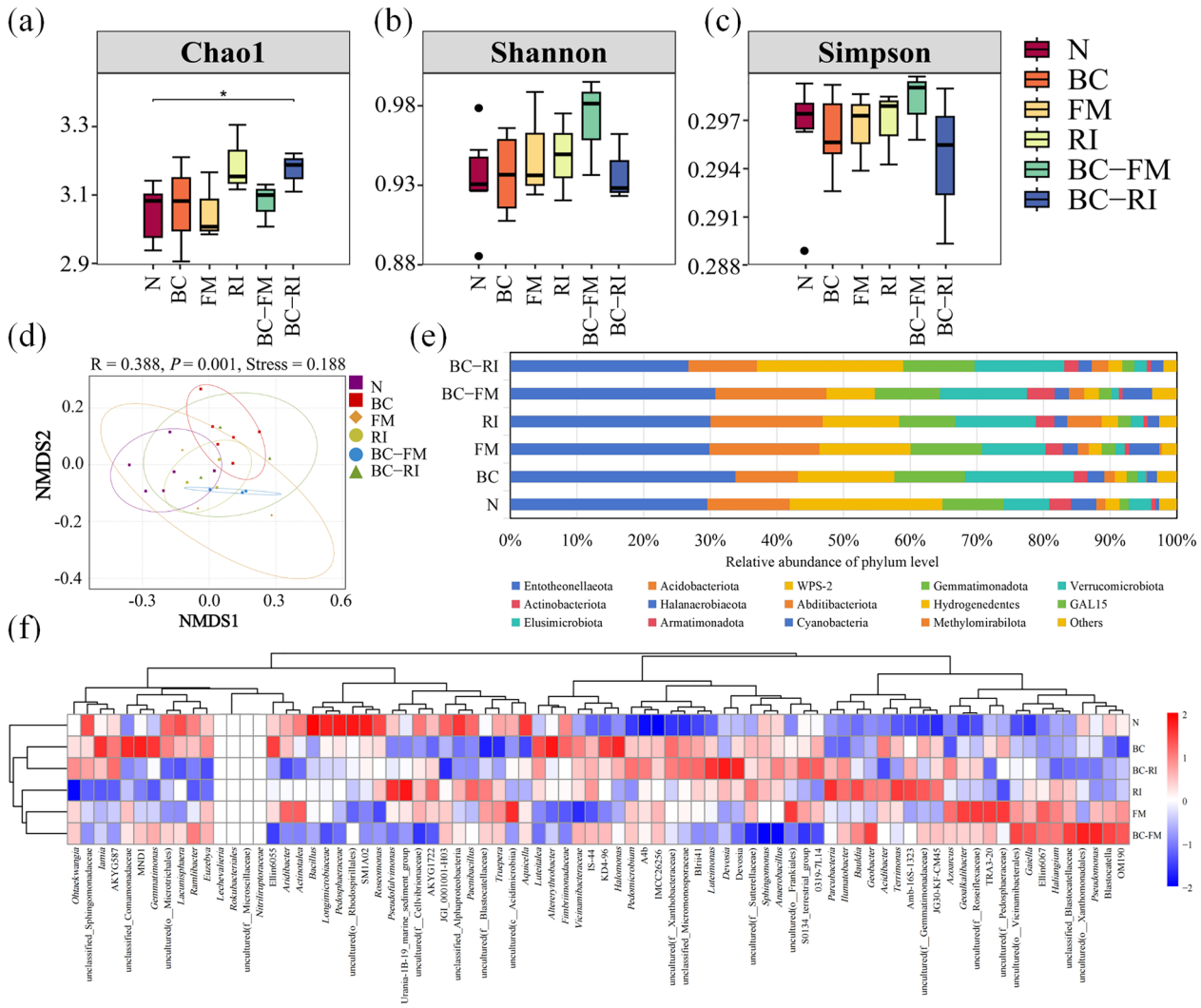

Fig. 6 Rhizosphere microbial (**a**–**c**) alpha diversity: Chao1, Shannon, Simpson indices; **d** NMDS ordination (Bray–Curtis distance); **e** phylum-level relative abundance (Top 10); **f** genus-level cluster heatmap (relative abundance > 1%). Treatments and statistical notations as in Fig. 2

sulfate-reducer potentially involved in As immobilization (Chen et al. 2025b; Yuan et al. 2025).

3.6 Correlation analysis unveils key plant–soil–microbe interactions

Mantel tests and structural equation modeling (Fig. S4) revealed key relationships that underpin the differential effectiveness of the BC–FM and BC–RI treatments (Fig. S4). The most robust pattern was the strong positive correlation between plant antioxidant defense (leaf CAT activity) and photosynthetic performance (Pn) ($r > 0.4$, $p < 0.01$). This statistical link provides strong support for the physiological model, wherein BC–FM enhances carbon assimilation by concurrently boosting oxidative stress tolerance.

Notably, several keystone microbial taxa showed significant correlations with critical soil and plant parameters. For instance, *Longimicrobiaceae* was positively correlated with both plant growth (e.g., biomass, $r = 0.13$) and SOC accumulation ($r = 0.16$), reinforcing its potential role in the carbon sequestration pathway driven by the BC–FM system. Conversely, *Lechevalieria* was significantly associated with enhanced microbial diversity (Shannon index, $r = 0.26$) and plant growth ($r = 0.16$), which aligns with the diverse and productive rhizosphere environment fostered by BC–RI.

In summary, these targeted correlations statistically validate the core premise of our study: the two biochar–AMF assemblies facilitate plant growth and soil remediation through distinct, microbe-mediated pathways. The

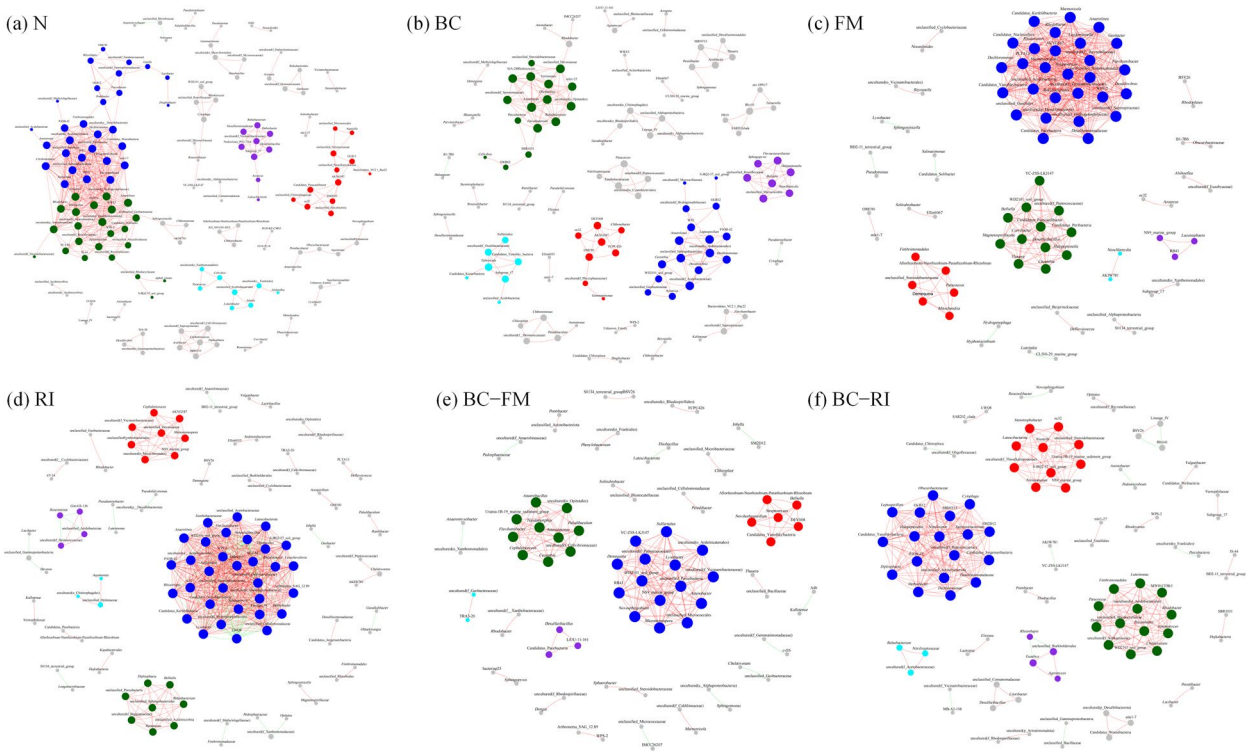

Fig. 7 Co-occurrence networks of rhizosphere microbial communities (genus-level OTUs, relative abundance > 0.1%). Edges represent significant correlations ($|r| \geq 0.4$, $p < 0.05$). The five largest clusters are indicated in the figure, colored dark blue, green, red, purple and light blue, respectively, in order of decreasing size. Treatments as in Fig. 1

BC–FM synergy is closely linked to carbon-driven processes and antioxidant enhancement, while the BC–RI synergy is tied to the activation of a more diverse microbiome. Collectively, these findings provide a mechanistic basis for the observed "fungal species–metal valency matching pattern".

4 Conclusion

This study deciphers the multipath synergy of biochar-loaded AMF in red mud remediation by integrating plant physiology, soil chemistry, and microbial ecology. The key conclusions are threefold: (1) Functional Specificity: The two biochar–AMF assemblies, BC–FM and BC–RI, differentially enhanced *A. donax* resilience under RM stress. BC–FM boosted photosynthesis and catalase-driven antioxidant defense, while BC–RI prioritized biomass accumulation and peroxidase activation; (2) Valency-Matched Remediation: The core finding validates a "fungal species–heavy metal valency matching" principle. BC–FM preferentially immobilized the oxyanion arsenate (As(V)) by reducing its exchangeable fraction, making it ideal for As-risk zones. Conversely, BC–RI targeted the cationic lead (Pb (II)), effectively reducing total soil Pb, making it superior for Pb-contaminated areas; (3) Soil Health Recovery: Both systems concurrently mitigated saline-alkaline stress and enhanced nutrient cycling. BC–FM drove soil organic carbon accumulation, while BC–RI unlocked phosphorus and enriched microbial diversity, collectively reactivating soil biological functions.

Based on these findings, we propose a practical compartmentalized remediation strategy: BC–RI for Pb/salinity-dominated areas and BC–FM for As-risk zones. Future efforts should first validate this strategy in the field, evaluating long-term AMF survival, biochar stability, and economic viability. Simultaneously, mechanistic studies using techniques such as XPS and organic acid profiling are needed to directly confirm the valency-specific detoxification pathways proposed herein.

Supplementary Information

The online version contains supplementary material available at https://doi.org/10.1007/s42773-025-00568-7.

Supplementary material 1.

Acknowledgements
This work was supported by the National Natural Science Foundation of China (No. 32460312). We want to acknowledge editor and anonymous reviewers for their valuable comments.

Author contributions
Xiaohui Wang: Supervision, conceptualization, methodology, formal analysis, resources, funding acquisition, writing—original draft. Yingqiang Sun: Investigation, data analysis, writing—original draft. Danjuan Zeng, Chuanming Fu, Keyi Wang: Formal analysis, data analysis. Junbo Yang, Jianxiong Liao: Reviewing the manuscript. Kanghua Xian: Investigation. Fuqiang Song, Gaozhong Pu: Supervision, Conceptualization, Methodology, Formal analysis, Resources, Funding Acquisition. All authors read and approved the final manuscript.

Funding
The authors are grateful for the financial support of the National Natural Science Foundation of China (32460312), the National Natural Science Foundation of Guangxi (2025GXNSFBA069005, 2025GXNSFAA069855), the Key Project of Natural Science Foundation of Heilongjiang Province (ZD2024C006), the Fundamental Research Fund of the Guangxi Institute of Botany, China (Guizhiye, 24010), and the Key R&D Program of Guangxi, China (Guike AB22035038).

Data availability
Data will be made available on reasonable request.

Declarations

Ethics approval and consent to participate
Not applicable.

Consent for publication
Not applicable.

Competing interests
On behalf of all authors, the corresponding author states that there is no competing interests.

Author details
[1]Guangxi Key Laboratory of Plant Conservation and Restoration Ecology in Karst Terrain, Guangxi Institute of Botany, Guangxi Zhuang Autonomous Region and Chinese Academy of Sciences, Guilin 541006, China. [2]School of Resources, Environment and Materals, Guangxi University, Nanning 530004, China. [3]Engineering Research Center of Agricultural Microbiology Technology, Ministry of Education, Heilongjiang Provincial Key Laboratory of Ecological Restoration and Resource Utilization for Cold Region, Heilongjiang University, Harbin 150080, Heilongjiang, China.

Received: 2 August 2025 Revised: 23 December 2025 Accepted: 25 December 2025
Published online: 13 February 2026

References

Alshaal T, Domokos-Szabolcsy É, Márton L, Czakó M, Kátai J, Balogh P, Elhawat N, El-Ramady H, Fári M (2013) Phytoremediation of bauxite-derived red mud by giant reed. Environ Chem Lett 11(3):295–302
Babzada SA, Raja V, Bhat AH, Qadir SU, Radhakrishnan A, Kumar N, Alsahli AA, Ahmad P (2024) Alleviation of salinity stress by EDTA chelated-biochar and arbuscular mycorrhizal fungi on maize via modulation of antioxidants activity and biochemical attributes. J Hazard Mater 24(1):63
Cappuyns V, Swennen R, Niclaes M (2007) Application of the BCR sequential extraction scheme to dredged pond sediments contaminated by Pb–Zn mining: a combined geochemical and mineralogical approach. J Geochem Explor 93(2):78–90
Chandra P, Singh A, Prajapat K, Rai AK, Yadav RK (2022) Native arbuscular mycorrhizal fungi improve growth, biomass yield, and phosphorus nutrition of sorghum in saline and sodic soils of the semi-arid region. Environ Exp Bot 201:104982
Chen YL, Yang WT, Liu HY, Mao WJ, Zhang J, Wang B, Yang LY, Wang SS, Zhou H, Zeng P, Wu P (2025a) Phosphorus-loaded magnetic biochar for remediation of cadmium contaminated paddy soil: efficacy and identification of limiting factors. J Hazard Mater 492:138162
Chen RA, Chai XQ, Zhang YX, Zhou TX, Xia YY, Jiang XJ, Lv B, Zhang J, Zhou LX, Tian X, Wang RA, Mao LJ, Zhao F, Zhang HY, Hu J, Qiu JF, Zou Z, Chen CZ (2025b) Novel role of FTO in regulation of gut-brain communication via *Desulfovibrio fairfieldensis*–produced hydrogen sulfide under arsenic exposure. Gut Microbes 17:2438471
Deng SG, Yang YF, Hu CY, Xiao SF, Kuzyakov Y, Liu CJ, Ma LQ (2025) Arsenic uptake and metabolism in mycorrhizal As-hyperaccumulator *Pteris vittata*: symbiotic p transporters and as reductases. Environ Sci Technol 59(11):5556–5567
Di Carlo E, Boullemant A, Courtney R (2019a) A field assessment of bauxite residue rehabilitation strategies. Sci Total Environ 663:915–926
Di Carlo E, Boullemant A, Courtney R (2019b) Ecotoxicological risk assessment of revegetated bauxite residue: implications for future rehabilitation programmes. Sci Total Environ 698:134344
Dou ZW, Sun YH, Zhang YH, Wang MX, Zhang N, Liu AJ, Hu XX (2024) Amelioration of the physicochemical properties enhanced the resilience of bacteria in bauxite residues. J Hazard Mater 471:134455
Essahibi A, Benhiba L, Fouad MO, Babram MA, Ghoulam C, Qaddoury A (2019) Responsiveness of carob (*Ceratonia siliqua* L.) plants to arbuscular mycorrhizal symbiosis under different phosphate fertilization levels. J Plant Growth Regul 38(4):1243–1254
Feng ZW, Liu XD, Qin YQ, Feng GD, Zhou Y, Zhu HH, Yao Q (2023) Cooperation of arbuscular mycorrhizal fungi and bacteria to facilitate the host plant growth dependent on soil pH. Front Microbiol 14:1116943
Gao JF (2006) Experimental guidance for plant physiology. Higher Education Press, Beijing
Garg N, Cheema A (2021) Relative roles of arbuscular mycorrhizae in establishing a correlation between soil properties, carbohydrate utilization and yield in *Cicer arietinum* L. under As stress. Ecotoxicol Environ Saf 207:111196
Glinska S, Gapinska M (2013) The effect of pre-incubation of *Allium cepa* L. roots in the ATH-rich extract on Pb uptake and localization. Protoplasma 250(2):601–611
Gujre N, Agnihotri R, Rangan L, Sharma MP, Mitra S (2021) Deciphering the dynamics of glomalin and heavy metals in soils contaminated with hazardous municipal solid wastes. J Hazard Mater 416:125869
Hao SY, Tian Y, Lin ZQ, Xie LZ, Zhou XB, Bañuelos GS (2024) Effects of arbuscular mycorrhizal fungi on the reduction of arsenic accumulation in plants: a meta-analysis. Front Plant Sci 15:1327649
He XX, Chen YQ, Liu SJ, Gunina A, Wang XL, Chen W, Shao YH, Shi LL, Yao Q, Li JX, Zou XM, Schimel JP, Zhang WX, Fu SL (2018) Cooperation of earthworm and arbuscular mycorrhizae enhanced plant N uptake by balancing absorption and supply of ammonia. Soil Biol Biochem 116:351–359
Hobbie EA, Jocher G, Peichl M, Zhao P, Zhou ZX, Hasselquist NJ (2025) Ectomycorrhizal hydrophobicity and host association influence ectomycorrhizal C dynamics, N dynamics, and fruiting patterns in N addition experiments under pine. Plant Soil 511(1–2):867–883
Lang M, Li X, Zheng CY, Li HG, Zhang JL (2021) Shading mediates the response of mycorrhizal maize (*Zea mays* L.) seedlings under varying levels of phosphorus. Appl Soil Ecol 166:104060
Li TT, Yang H, Zhang NL, Dong LJ, Wu AP, Wu QQ, Zhao MS, Liu H, Li Y, Wang YH (2023) Synergistic effects of arbuscular mycorrhizal fungi and biochar are highly beneficial to *Ligustrum lucidum* seedlings in Cd-contaminated soil. Environ Sci Pollut Res Int 30(45):11214–11227
Li GH, Liu JJ, Yi LY, Luo J, Jiang T (2024) Bauxite residue (red mud) treatment: current situation and promising solution. Sci Total Environ 948:174757
Li YL, Wu SJ, Jin ZX, Li JM (2025) Differential strategies of two arbuscular mycorrhizal fungi varieties in the protection of *Lycium ruthenicum* under saline-alkaline stress. Plant Physiol Biochem 222:109725
Liu Y, Hu TS, Zhu R, Chen QW, Zeng X, Jing PR, Huang YF (2025a) A stomatal optimization model integrating leaf stomata–photosynthetic capacity regulation in response to soil water stress. Agric Water Manage 308:109285
Liu YW, Guan DX, Qiu LX, Luo Y, Liu F, Teng HH, Kuzyakov Y, Ma LQ (2025b) Spatial dynamics of phosphorus mobilization by mycorrhiza. Soil Biol Biochem 206:109797
Ma PK, Shi ZQ, Diao FW, Hao LJ, Zhang JX, Xu J, Wang LX, Dang ZH, Guo W (2021) Effects of arbuscular mycorrhizal fungi on growth and Na plus accumulation of *Suaeda glauca* (Bunge) grown in salinized wetland soils. Appl Soil Ecol 166:104065

Nirukshan GS, Ranasinghe S, Sleutel S (2023) The effect of biochar on mycorrhizal fungi mediated nutrient uptake by coconut (*Cocos nucifera* L.) seedlings grown on a Sandy Regosol. Biochar 4:68

Rijk I, Ekblad A, Dahlin AS, Enell A, Larsson M, Leroy P, Kleja DB, Tiberg C, Hallin S, Jones C (2024) Biochar and peat amendments affect nitrogen retention, microbial capacity and nitrogen cycling microbial communities in a metal and polycyclic aromatic hydrocarbon contaminated urban soil. Sci Total Environ 936:173454

Robinson C, Schinner F, Ohlinger R, Kandeler E, Margesin R (1995) Methods in soil biology. J Ecol 85(3):404

Sarathambal C, Khankhane PJ, Gharde Y, Kumar B, Varun M, Arun S (2017) The effect of plant growth—promoting rhizobacteria on the growth, physiology, and Cd uptake of *Arundo donax* L. Int J Phytoremediation 19(4):360–370

Seshadri B, Bolan NS, Naidu R (2015) Rhizosphere–induced heavy metal(loid) transformation in relation to bioavailability and remediation. J Plant Nutr Soil Sci 178(2):524–548

Souza T, dos Santos JBL, Batista DS (2025) Hydrogel and arbuscular mycorrhizal fungi inoculation as soil conditioners in dark Earth of the *Amazon rainforest*. J Soil Sediment 25(5):1487–1496

Sun SK, Chen J, Zhao FJ (2023) Regulatory mechanisms of sulfur metabolism affecting tolerance and accumulation of toxic trace metals and metalloids in plants. J Exp Bot 74(11):3286–3299

Tóth C, Simon L, Tóth B (2024) Microanatomical changes in the leaves of *Arundo donax* (l.) caused by potentially toxic elements from municipal sewage sediment. Plants 13(5):740

Videgain-Marco M, Marco-Montori P, Martí-Dalmau C, Jaizme-Vega MD, Manya-Cervello JJ, Garcia-Ramos FJ (2021) The effects of biochar on indigenous arbuscular mycorrhizae fungi from agroenvironments. Plants-Basel 10(5):950

Wang XH, Wang Y, Sun YQ, Wang KY, Yang JB, Zeng DJ, Mo L, Liao JX, Peng QS, Yao Y, Pu G (2025) Soil polluted system shapes endophytic fungi communities associated with *Arundo donax*: a field experiment. PeerJ 13:e18789

Wen YQ, Wu RT, Xu TL, Cao RR, Song G, Qi DD, Chang W, Li K, Ping Y, Zhang MM, Fan XX, Song FQ (2025) AMF and biochar reshape the bacterial network in rhizosphere soil of *Ricinus communis* under chromium (Cr) stress and improve soil quality. J Hazard Mater 492:138122

Xian KH, Su J, Fu CM, Huang NZ, Gong QF, He JX (2018) Techniques for rapid propagation of *Arundo donax*. Guihaia 38(1):128–134

Xie KH, Chen YX, Wang XQ, Zhou XY, Cheng YZ, Yu XC, Wang J, Sun MT, Li YS, He CX (2025) Physiological and multi-omics analysis revealed the mechanism of arbuscular mycorrhizal fungi to cadmium toxicity in green onion. Ecotox Environ Safe 290:117754

Yang ZM, Zou ZD, Akhtar MA, Niu WJ, Ren LN, Zhang S, Liu N, Cao HL (2021) Synergistic effects of N–containing heterocyclic and Ca ligand structures on the phosphorus adsorption of N/Ca co-doped biochar. J Clean Prod 485:144392

Yang JB, Wang XH, Wang KY, Zeng DJ, Mo L, Li S, Fang BZ, Rekadwad B, Li WJ, Pu GZ (2025) Mature Tiankengs are biodiversity hotspots of soil microorganisms in the karst region. Ecol Indic 170:113034

Yuan XF, Deng YM, Gao J, Zheng TL, Xu YX, Wang YX (2025) Unveiling the role of sulfate—reducing bacteria in arsenic methylation in alluvial-lacustrine aquifers. Water Res 283:123864

Zaman QU, Guo LH, He XR, Luo Y, Liu C, Murtaza G, Sultan K, Fahad S, Cheng X, Ashraf K, Deng G (2025) Synergistic effect of arbuscular mycorrhizal fungi, biochar and seaweed extract for improving the copper tolerance in hemp. Ind Crop Prod 224:120358

Zhang D, Jiang QW, Liang DY, Huang SX, Liao JX (2021) The potential application of giant reed (*Arundo donax*) in ecological remediation. Front Env Sci-Switz 9:652367

Zhang XL, Qiu YP, Gilliam FS, Gillespie CJ, Tu C, Reberg-Horton SC, Hu SJ (2022) Arbuscular mycorrhizae shift community composition of N-cycling microbes and suppress soil N2O emission. Environ Sci Technol 56(18):13461–13472

Zheng X, Li A, Nie RN, Wu CX, Ji XY, Tang JL, Zhang JP (2024) Differential strategies of two arbuscular mycorrhizal fungi varieties in the protection of *Lycium ruthenicum* under saline-alkaline stress. J Fungi 10(8):554

Zhou HY, Nian FZ, Chen BD, Zhu YG, Yue XR, Zhang NM, Xia YS (2023) Synergistic reduction of arsenic uptake and alleviation of leaf arsenic toxicity in maize (*Zea mays* L.) by arbuscular mycorrhizal fungi (AMF) and exogenous iron through antioxidant activity. J Fungi 9(6):677

Zhu SX, Zhao W, Sun SX, Yang XQ, Mao H, Sheng LY, Chen ZB (2024) Metagenomic analysis revealed N-metabolizing microbial response of *Iris tectorum* to Cr stress after colonization by arbuscular mycorrhizal fungi. Ecotoxicol Environ Saf 273:116157